Protein Structure and Folding:

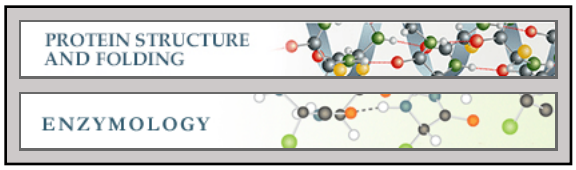

Insights into the Reaction of Protein-tyrosine Phosphatase 1B: CRYSTAL STRUCTURES FOR TRANSITION STATE ANALOGS OF BOTH CATALYTIC STEPS

Tiago A. S. Brandão, Alvan C. Hengge and Sean J. Johnson

J. Biol. Chem. 2010, 285:15874-15883.
doi: 10.1074/jbc.M109.066951 originally published online March 16, 2010

THE JOURNAL OF BIOLOGICAL CHEMISTRY VOL. 285, NO. 21, pp. 15874–15883, May 21, 2010

Insights into the Reaction of Protein-tyrosine Phosphatase 1B

CRYSTAL STRUCTURES FOR TRANSITION STATE ANALOGS OF BOTH CATALYTIC STEPS[*S]

Received for publication, September 17, 2009, and in revised form, March 3, 2010 Published, JBC Papers in Press, March 16, 2010, DOI 10.1074/jbc.M109.066951

Tiago A. S. Brandão[1], **Alvan C. Hengge**[2], **and Sean J. Johnson**[3]

From the Department of Chemistry and Biochemistry, Utah State University, Logan, Utah 84322-0300

Catalysis by protein-tyrosine phosphatase 1B (PTP1B) occurs through a two-step mechanism involving a phosphocysteine intermediate. We have solved crystal structures for the transition state analogs for both steps. Together with previously reported crystal structures of apo-PTP1B, the Michaelis complex of an inactive mutant, the phosphoenzyme intermediate, and the product complex, a full picture of all catalytic steps can now be depicted. The transition state analog for the first catalytic step comprises a ternary complex between the catalytic cysteine of PTP1B, vanadate, and the peptide DADEYL, a fragment of a physiological substrate. The equatorial vanadate oxygen atoms bind to the P-loop, and the apical positions are occupied by the peptide tyrosine oxygen and by the PTP1B cysteine sulfur atom. The vanadate assumes a trigonal bipyramidal geometry in both transition state analog structures, with very similar apical O–O distances, denoting similar transition states for both phosphoryl transfer steps. Detailed interactions between the flanking peptide and the enzyme are discussed.

The phosphorylation of tyrosine residues by protein-tyrosine kinases and the reverse action by protein-tyrosine phosphatases (PTPs)[4] is a common mechanism for the control of biological pathways (1–3). Protein-tyrosine phosphatase 1B (PTP1B) is a biomedically important phosphatase with several roles, including negative regulation of insulin signaling by dephosphorylation of the insulin receptor tyrosine kinase (4). Knock-out studies show that loss of PTP1B is associated with an increased insulin sensitivity and suppression of weight gain in mice (5). As a result, this enzyme has been considered a significant target for treatment of type 2 diabetes and obesity (6, 7). PTP1B also down-regulates cell growth by dephosphorylating the epidermal growth factor receptor (8). Overexpression has been observed in human breast and ovarian cancer, where it is believed to suppress potential tumors by antagonizing signaling of oncogenic factors (9, 10). Other PTPs are known virulence factors for a number of human diseases (11–13).

Reactions catalyzed by PTPs take place by a ping-pong mechanism (Fig. 1) (2). In the first step, a nucleophilic cysteine thiolate attacks the phosphate ester moiety of the substrate, resulting in formation of a phosphoenzyme intermediate with release of the peptidyl tyrosine. The second step occurs via attack of water on the phosphoenzyme intermediate and yields the final products inorganic phosphate and the regenerated enzyme. The central binding site for the substrate is the P-loop, a region at the bottom of a pocket that includes the nucleophilic cysteine and backbone amide groups oriented in a horseshoe fashion. The amide protons in the P-loop, together with a conserved arginine residue, hydrogen-bond to the phosphoryl group of the substrate and orient it for nucleophilic attack, providing transition state (TS) stabilization. Substrate binding is followed by conformational changes that culminate with closure of the active site pocket by a conserved and flexible loop of sequence WPD. The aspartic acid in this loop functions as a general acid in the first step and as a general base catalyst in the second step.

The design of PTP inhibitors is a very active area of research. A common strategy is focused on the synthesis of competitive inhibitors that block the active site (6, 11, 14). Binding affinities in these cases range from millimolar to micromolar, and specificity is often compromised by the high similarity between PTP active sites. In order to achieve more potency and selectivity, more extensive interactions are achieved by using doubly targeted inhibitors (9). For example, in PTP1B, targeting of a second Tyr(P) binding site in the vicinity of the active site has been used. In such cases, inhibition constants can be improved to the nanomolar range (15), and selectivity is gained because the second Tyr(P) site in PTP1B is not conserved among all PTPs.

One important reason for the limited success of single site inhibition in PTPs is the fact that substrate binding is far surpassed by the affinity of the TS. Like other PTPs, PTP1B catalyzes the hydrolysis of phosphate ester dianions, which have very slow rates of uncatalyzed hydrolysis (*e.g.* the half-life for the uncatalyzed attack of water on the dianion of alkyl phosphate esters is $\sim 1.1 \times 10^{12}$ years ($k = 2 \times 10^{-20}$ s^{-1} at 25 °C)) (16). Catalytic efficiency is achieved by selective affinity for the TS relative to the substrate. According to the TS binding paradigm, TS affinity is equivalent to the ratio between the specificity constant (k_{cat}/K_m) for the catalyzed reaction and its uncatalyzed rate constant (17). Based on kinetic constants for catalyzed (18) and uncatalyzed (16) reactions (see supplemental material), PTP1B exhibits transition state (TS) affinities of $>10^{13}$ M^{-1} for *p*-nitrophenyl phosphate (*p*NPP) and 10^{19} M^{-1}

* This work was supported, in whole or in part, by National Institutes of Health Grant GM47297 (to A. C. H.).

[S] The on-line version of this article (available at http://www.jbc.org) contains supplemental Table S1 and Figs. S1–S5.

The atomic coordinates and structure factors (codes 3I7Z and 3I80) have been deposited in the Protein Data Bank, Research Collaboratory for Structural Bioinformatics, Rutgers University, New Brunswick, NJ (http://www.rcsb.org/).

[1] Recipient of a fellowship from Coordenação de Aperfeiçoamento de Pessoal de Nível Superior (Brazil).

[2] To whom correspondence may be addressed. Tel.: 435-797-3442; Fax: 435-797-3390; E-mail: alvan.hengge@usu.edu.

[3] To whom correspondence may be addressed. Tel.: 435-797-2089; Fax: 435-797-3390; E-mail: sean.johnson@usu.edu.

[4] The abbreviations used are: PTP, protein-tyrosine phosphatase; TS, transition state; *p*NPP, *p*-nitrophenyl phosphate; KIE, kinetic isotope effect; bis-tris, 2-[bis(2-hydroxyethyl)amino]-2-(hydroxymethyl)propane-1,3-diol; MC, Michaelis complex; PDB, Protein Data Bank.

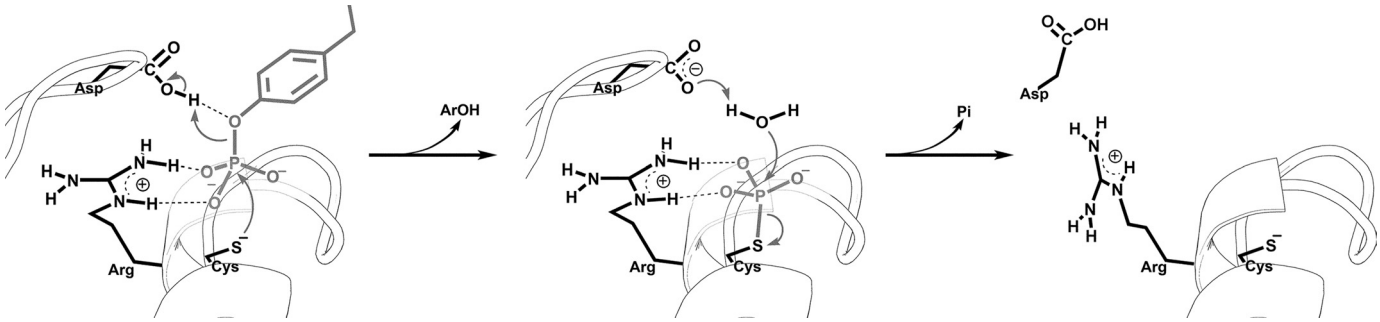

FIGURE 1. **The general mechanism of the PTP-catalyzed reaction.**

when the substrate is the peptide acetyl-DADEpYL-NH_2. Besides the known closure of the WPD-loop, the existence of other catalysis-associated conformational changes that might affect protein-substrate interactions is uncertain.

In order to better understand structural changes associated with catalysis, we have crystallized transition state analogs for the first and second catalytic steps. Kinetic isotope effects (KIEs) for the reaction of *p*-nitrophenyl phosphate by PTP1B were measured to verify that its transition state structure is similar to those of other PTPs. The first step TS analog reported here is a ternary complex that involves a central metavanadate with two apical ligands, the nucleophilic cysteine thiolate and the phenol leaving group, the latter as the tyrosyl oxygen atom in the peptide sequence DADEYL. This peptide is a fragment of the epidermal growth factor receptor, which, in phosphorylated form, exhibits strong affinity for PTP1B (18). A previous crystallographic study shows a Michaelis complex between a catalytically inactive C215S mutant of PTP1B and the phosphopeptide DADEpYL (19). The second step TS analog reported here is a complex between PTP1B and orthovanadate. Although a related structure has been previously described (18), the coordinates are not publicly available, and it was therefore necessary to determine a new structure approximating the second transition state. Comparisons of these newly determined and previously reported structures highlight significant protein conformational changes arising during catalysis.

These TS analogs are based on vanadate ions, which are tetrahedral in solution but in active sites of PTPs form stable pentavalent structures exhibiting trigonal bipyramid geometries (18, 20–23). Such structures are widely accepted as sharing close structural characteristics with the metaphosphate-like transition state in phosphate transfer (24). In comparison with other analogs (25–27), such as WO_4^{2-}, MgF_3^-, and NO_3^-, complexes based on vanadate have the advantage of displaying the same overall charge as phosphate and can easily derivatize and interact with ligands at their axial positions.

The new TS analog structures, together with previously solved structures of the apoenzyme (28), phosphoenzyme intermediate (29), and product complex (30), now provide a depiction of all of the catalytic steps involved in the mechanism of PTP1B. This full array of structures permits a step-by-step description of the structural changes involved in binding and catalysis, particularly those related to the following protein segments: 1) the P-loop (residues 215–222), which includes the nucleophilic cysteine (Cys^{215}) and an important serine (Ser^{222}) that stabilizes its thiolate form, and the arginine (Arg^{221}) involved in binding and transition state stabilization; 2) the WPD-loop (residues 179–187), bearing the general acid/base (Asp^{181}), which is active when this loop alternates from the open to the closed conformation; 3) the Q-loop (residues 261–262), including the residue Gln^{262}, an important player in the second catalytic step; 4) the lysine loop (residues 119–121), containing Lys^{120}, a conserved residue involved in key interactions with the WPD-loop (31); and 5) the Tyr(P) recognition loop (residues 47–49), involved in substrate recognition and binding.

EXPERIMENTAL PROCEDURES

The expression and purification of wild type PTP1B were slightly modified from previously reported methods (32) (see supplemental material). Protein concentrations were monitored by UV using an $A_{1\ mg/ml}^{280\ nm} = 1.24$. The peptide DADEYL (>98% pure) was a custom synthesis by Anaspec. Labeled and natural abundance *p*NPP (dicyclohexylammonium salt) were synthesized according to previous methods (33). Sodium orthovanadate (Na_3VO_4) was purchased from Fisher.

Kinetic Isotope Effect Determinations—KIEs were measured using the internal competition method and thus are isotope effects on *V*/*K* (34). In the commonly used notation, a leading superscript of the heavier isotope is used to indicate the isotope effect on the following kinetic quantity (*e.g.* $^{15}(V/K)$ denotes $^{14}(V/K)/^{15}(V/K)$, the nitrogen-15 KIE on *V*/*K*).

Natural abundance *p*NPP was used for measurements of $^{15}(V/K)$. The ^{18}O KIEs $^{18}(V/K)_{bridge}$ and $^{18}(V/K)_{nonbridge}$ were measured by the remote label method, using the nitrogen atom in *p*-nitrophenol as a reporter for isotopic fractionation in the labeled oxygen positions (35). The isotopic isomers used are shown in the supplemental material. Isotope effect determinations were made at 25 °C in 50 mM bis-tris buffer, pH 5.5, containing 1 mM dithiothreitol. The *p*NPP concentration was 18 mM, and the reaction was started by the addition of wild type PTP1B to a final concentration of 0.21 μM. Within 15–20 min, the reactions reached 40–60% completion and were stopped by titrating with HCl to pH 2–3. Protocols for isolation of *p*-nitrophenol and isotopic analysis and calculation of the isotope effects were the same as previously described (36) and are described in the supplemental material.

Crystallization—Crystals were grown using sitting drop vapor diffusion at 4 °C by mixing 2 μl of protein solution, 0.5 μl of 30% (w/v) sucrose, and 3 μl of precipitant solution (0.1 M Hepes, pH 7.5, 0.2 M magnesium acetate, and 15–17% polyethylene glycol 8000). Single crystals appeared after 3 days. The

protein solution was prepared as follows. 0.36 μl of 100 mM of Na_3VO_4 and 10 μl of 50 mM DADEYL peptide (at pH 8.5–9.0) were mixed and allowed to react for 1–1.5 h; 50 μl of native PTP1B (12 mg/ml in 10 mM Tris, pH 7.5, 25 mM NaCl, 0.2 mM EDTA, and 3 mM dithiothreitol) was then added to the peptide/vanadate mixture and immediately placed in the crystallization tray. The final protein solution contained a ratio of 1:3:30 between PTP1B, Na_3VO_4, and the peptide DADEYL. Crystallization at higher concentrations of Na_3VO_4 resulted in different crystal morphology; a 30:3 vanadate/peptide ratio gave crystals that proved to be a binary complex between PTP1B and VO_4^{3-}. Cryoprotection was performed by transferring crystals stepwise into stabilization solution with increasing glycerol amounts to a final concentration of 15% and the respective initial concentrations of ligands present in the protein solution, and then flash-cooled in liquid nitrogen.

Data Collection, Structure Determination, and Refinement—Diffraction data were collected using a home source generator and detector (Rigaku RU-200/Raxis IV++). Data were indexed and processed using d*TREK in the program Crystal Clear (37). Molecular replacement was performed using Phaser (38) from the CCP4 program suite (39, 40). The search model was the apo wild type PTP1B structure (Protein Data Bank (PDB) entry 2CM2) with the active site water molecules removed. Refinement was performed using the program Phenix (41). The TLS groups were generated by the TLS Motion Determination server (42). Coot (43) and MolProbity (44) were used for model building and validation. The crystallographic data and statistics of structure refinement are given in Table 1. The observed differences in *B*-factors between TSA1 (transition state analog 1) and TSA2 (TSA1 > TSA2) are due to tighter crystal packing along the *c* axis of the unit cell in TSA2. The bound peptide in TSA1 partially disrupts packing along the *c* axis, resulting in increased spacing and conformational flexibility between adjacent molecules. Structure factors and coordinates for the PTP1B-VO_3-DADEYL and PTP1B-VO_4 structures have been deposited in the PDB under accession numbers 3I7Z and 3I80, respectively. All figures depicting crystal structures were prepared using PyMOL (45).

RESULTS

Kinetic Isotope Effects—Reactions of wild type PTP1B with *p*NPP were carried out at the optimum pH of 5.5 and 25 °C, where $K_m = 0.58 \pm 0.01$ mM and $k_{cat} = 24.4 \pm 0.4\ s^{-1}$. The isotope effect data are shown in Table 2. As the enzymatic substrate of PTPs is the dianionic form of *p*NPP, the $^{18}(V/K)_{nonbridge}$ isotope effect was corrected considering the isotope fractionation for protonation of the nonbridge oxygen atoms because *p*NPP is present as a mixture of monoanion and dianion forms at this pH. Data for the reaction catalyzed by the other PTPs YopH from *Yersinia* and rat PTP1 are also shown (36) for comparison purposes.

Crystallography—The two transition state analogs were crystallized under similar conditions, except for the concentrations of peptide and vanadate, which were optimized to give the structures of the transition state analog for the first step (TSA1) and the second step (TSA2). With a ratio of peptide/vanadate/enzyme of 3:30:1, hexagonal prism crystals were obtained. The composite omit map of the active site revealed electronic density for a single vanadate, exhibiting a trigonal bipyramidal structure conforming to TSA2, and the map showed no evidence for a bound peptide. When the peptide/vanadate ratio was 30:3, crystals grew with hexagonal bipyramidal morphology. Composite omit maps for the active site reveal clear electronic density for the vanadyl-peptide complex and a trigonal bipyramid structure that is consistent with TSA1. Supplemental Fig. S2 displays composite omit maps for residues in the active site of TSA1 and TSA2.

Fig. 2 shows key active site interactions in the TS analog structures. The apical positions of the vanadate moieties of both TSA1 and TSA2 are occupied by the sulfur of Cys^{215} and by an oxygen atom at distances of 2.5 and 2.1 Å, respectively, from the central vanadium atom. The equatorial oxygen atoms hydrogen-bond to backbone amide groups of the P-loop and

TABLE 1

Data collection and refinement statistics for the PTP1B transition state analogs

Values in parentheses correspond to those in the outer resolution shell.

	PTP1B-VO_3-DADEYL (TSA1)	PTP1B-VO_4 (TSA2)
Data collection		
Beamline	Home source	Home source
Wavelength (Å)	1.5418	1.5418
Resolution range (Å)	29.43–2.30	38.04–2.25
Outer shell (Å)	2.38-2.30	2.33-2.25
No. of reflections		
Unique	24,185	22,453
Total	135,032	89,995
Average redundancy	5.6 (5.6)	4.0 (4.0)
Mean $I/\sigma(I)$	9.2 (2.3)	8.6 (2.2)
Completeness (%)	99.9 (100.0)	100.0 (99.9)
R_{sym} (%)[a]	7.5 (54.0)	8.4 (47.3)
Space group	P3121	P3121
Unit cell dimensions (*a*, *b*, *c* (Å); $\alpha = \beta = 90°$ and $\gamma = 120°$)	88.0, 88.0, 118.6	87.8, 87.8, 103.8
Refinement		
R_{work}/R_{free} (%)[b]	20.6/23.2	19.9/23.5
Atoms in the structure		
Protein	2482	2440
Waters	150	231
Ligands/ions	28	31
Average *B*-factors (Å^2)		
Protein	75.3	44.4
Water	66.8	53.0
Ligands/ions	100.1	64.4
Root mean square deviation bond (Å)/angle (degrees)	0.009/1.0	0.006/0.9
Protein geometry[c]		
Ramachandran outliers (%)	0.3	0.3
Ramachandran favored (%)	98.0	98.3
Rotamer outliers (%)	0.0	0.4
Protein Data Bank entry	3I7Z	3I80

[a] $R_{sym} = (\Sigma|(I - \langle I\rangle)|)/(\Sigma I)$, where $\langle I\rangle$ is the average intensity of multiple measurements.

[b] $R_{work} = (\Sigma||F_{obs}| - |F_{calc}||)/(\Sigma|F_{obs}|)$ and is calculated using all data; R_{free} is the *R*-factor based on 5% of the data excluded from refinement.

[c] Ramachandran statistics were calculated using the MolProbity server (44).

TABLE 2

Isotope effects for the catalyzed reaction of *p*NPP by the wild type enzymes PTP1B, PTP1, and YopH and the YopH general acid mutant

All were measured at the pH optimum for activity. Values in parentheses after KIE data are S.E. in the last decimal place.

Reaction	$^{15}(V/K)$	$^{18}(V/K)_{bridge}$	$^{18}(V/K)_{nonbridge}$
PTP1B wild type[a]	1.0004(2)	1.0121(9)	1.0018(5)
Rat PTP1[a] (36)	1.0001(2)	1.0142(4)	0.998(2)
YopH wild type[b] (36)	0.9999(3)	1.0152(6)	1.000(1)
YopH D356A[c] (36)	1.0022(3)	1.0274(8)	1.0007(5)

[a] pH 5.5 and 25 °C.

[b] pH 5.0 and 25 °C.

[c] pH 6.0 and 35 °C.

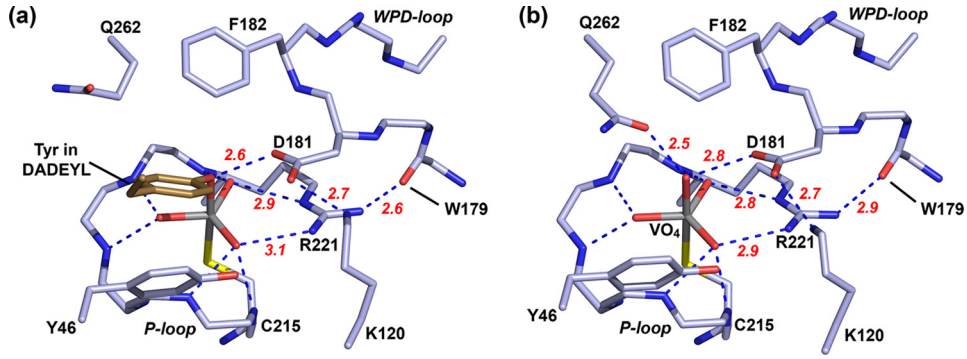

FIGURE 2. **Orientation of key residues at the active site of PTP1B and the binding environment for trigonal bipyramid structures in the transition state analogs.** *a*, first transition state complex (TSA1) between native PTP1B, metavanadate, and the Tyr in the peptide DADEYL; *b*, second transition state (TSA2) complex between native PTP1B and orthovanadate. The Trp^{179} ring was omitted for the sake of clarity, and only the backbone carbonyl group is shown. Hydrogen bond distances (in *red*) are in Å. See supplemental Fig. S2 for electron density surrounding residues at the active site of TSA1 and TSA2. Stereo images of *a* and *b* are included in supplemental Fig. S3.

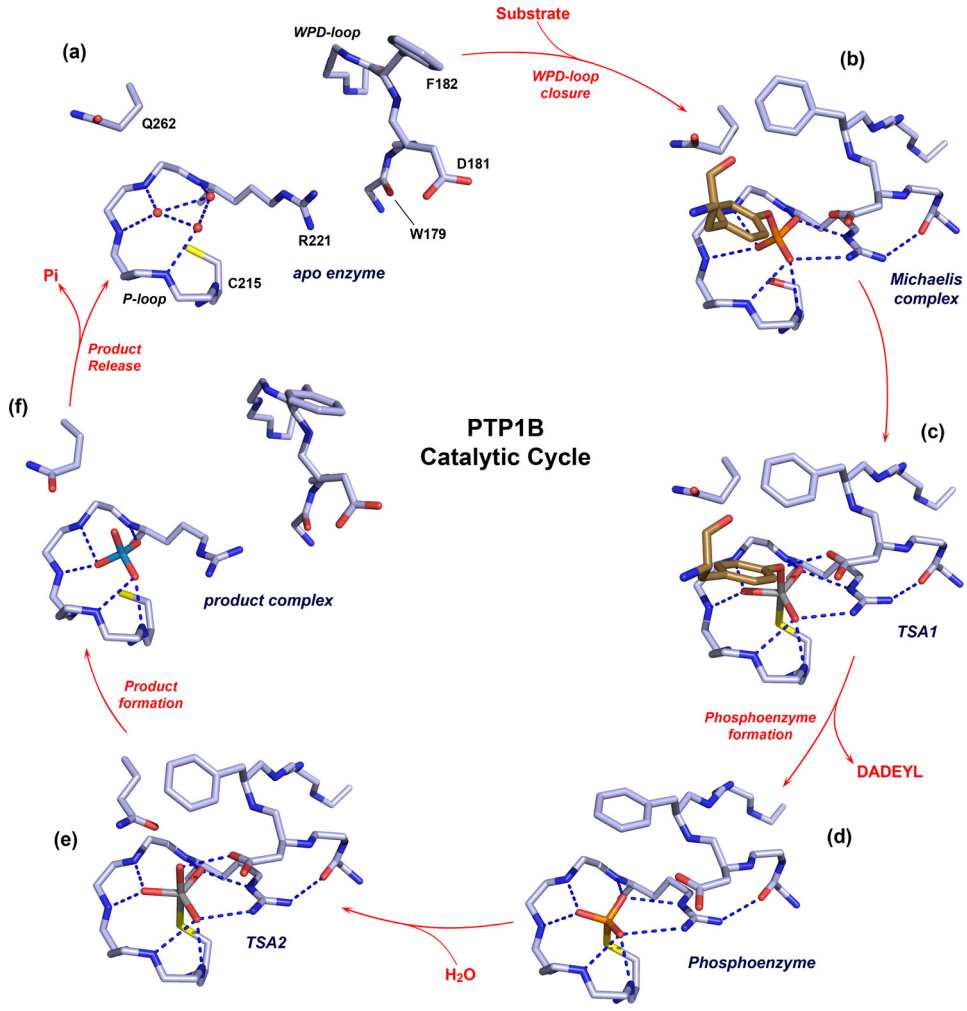

FIGURE 3. **Crystal structures along the pathway of the reaction catalyzed by PTP1B.** Hydrogen bond distances are in Å. The Trp^{179} ring was omitted for the sake of clarity, and only the backbone carbonyl group is shown. *a*, resting state PTP1B apoenzyme (PDB entry 2CM2) (28); *b*, Michaelis complex between PTP1B C215S and the peptide DADEpYL (PDB entry 1PTU) (19); *c*, first transition state complex between native PTP1B, metavanadate, and the Tyr in the peptide DADEYL (new structure, PDB entry 3I7Z); *d*, PTP1B Q262A cysteinyl-phosphate intermediate enzyme (PDB entry 1A5Y) (29); *e*, second transition state complex, between native PTP1B and orthovanadate (new structure, PDB entry 3I80); *f*, PTP1B-tungstate product analog complex (PDB entry 2HNQ) (30). These structures are further summarized in supplemental Table S1.

the guanidinium group of Arg^{221}, which is rotated in relation to the apo structure by about 82° around the χ-3 dihedral angle (see Fig. 3). Substrate and competitive inhibitors cause the same conformational change in Arg^{221} (19, 28, 46). In this conformation, the side chain of Arg^{221} hydrogen-bonds with the backbone carbonyl of Trp^{179} and assists the WPD-loop in a shift from the open, catalytically inactive to the closed, active conformation. This brings the WPD-loop residue Asp^{181} into proximity to protonate the leaving group oxygen (47). The essential role of this conserved arginine in facilitating WPD-loop closure has been shown in the closely related PTP YopH, where the R221K mutation disables general acid catalysis, presumably by affecting WPD-loop movement (33).

Gln^{262} in TSA1 occupies a similar position as in the Michaelis complex and is rotated 132° counterclockwise in relation to TSA2 (Fig. 2*b*). This residue is believed to position a nucleophilic water molecule in the second catalytic step (29). In TSA1, the amide proton of the side chain of Gln^{262} hydrogen bonds to the carbonyl oxygen of Gly^{259} (not depicted). The same interaction is observed in the apo and Michaelis complex. In TSA2, the side chain of Gln^{262} rotates into the active site, and the amide carbonyl oxygen hydrogen-bonds to the apical oxygen in the trigonal bipyramidal vanadate moiety.

In both TSA1 and TSA2 structures, Lys^{120} adopts a similar conformation, hydrogen-bonding to Asp^{181} and Glu^{115} at donor-acceptor distances of 2.6 and 2.7 Å, respectively. In the Michaelis complex, distances are 2.8 and 3.0 Å, respectively. In contrast, in the phosphoenzyme, the Lys^{120} side chain does not hydrogen-bond to other protein residues. This residue has been suggested to be part of dynamic events during substrate and inhibitor binding (31, 48). The K120A mutation has little effect on K_m and k_{cat} for *p*NPP hydrolysis and K_i values for vanadate (49). How-

ever, the use of a nonbiological substrate may preclude a proper definition of the role of this residue. In fact, protein alignments reveal that most PTPs retain a Lys or Arg at this position, suggesting an important role for this residue (50). The crystal structure of a complex between PTP1B and insulin receptor tyrosine kinase reveals that Lys^{120} is involved in a salt bridge interaction with insulin receptor tyrosine kinase (51).

Extensive interactions occur between the peptide of TSA1 and a surface groove adjacent to the active site (supplemental Fig. S4). These interactions include hydrogen bonds between the backbone amide proton of Arg^{47} in PTP1B and the backbone carbonyl oxygen of Asp^{-2} in the peptide and between the side chain carboxyl of Asp^{48} in PTP1B and the backbone amide protons of Tyr(P) and Leu^{+1} in the peptide.[5] Similar interactions are observed in the Michaelis complex along the core of the peptide, although positions of the peptide backbone and N-terminal residue side chains are slightly different. The change in position of the peptide backbone is accompanied by movement of the aryl ring of the substrate, which is about 0.45 Å farther away from the active site in TSA1 than in the Michaelis complex, as measured by the distance between the aryl ring and Cα of Arg^{221}. Differences in N-terminal regions of the peptides may arise from crystal packing. Hydrogen bonds along this region are observed with adjacent protein molecules; in TSA1, the side chain of Asp^{-4} hydrogen-bonds to the side chain of Thr^{168} in an adjacent molecule and to Arg^{47} in the same molecule. In the Michaelis complex structure, the respective aspartic acid hydrogen bonds to the backbone carbonyl of Gln^{166} in an adjacent molecule. There are no other significant changes in the enzyme or peptide between Michaelis complex and TSA1 structures that can be attributed to crystal packing.

Fig. 3 combines the present TS structures with published ones to depict the active site arrangement at each step of the pathway. Supplemental Table S1 summarizes the structures used for each step.

DISCUSSION

Kinetic Isotope Effects and Transition State Structure

The KIEs for PTP1B are similar to those reported previously for other PTPs (Table 2). Because they were measured using the competitive method, the isotope effects are on the kinetic quantity V/K, which includes events up to and including the first irreversible step. These thus reflect the first catalytic step, phosphoryl transfer from substrate to enzyme.

Kinetic isotope effects reflect differences in bonding to the labeled atom between the ground state and transition state (52). Consequently, they are useful in probing transition state structures and reaction mechanisms of reactions. A primary kinetic isotope effect at an atom undergoing bond cleavage will be normal (>1), due to the preference of the heavier isotope for the lower energy (more tightly bonded) position. Secondary kinetic isotope effects are normal when the labeled atom becomes more loosely bonded in the transition state or inverse (<1) when bonding becomes tighter. KIEs have been reported for a number of enzymatic and uncatalyzed phosphate ester reactions (35, 53–57), which provides a background for the interpretation of the KIE data measured in this work.

The three KIEs give different information regarding transition structure and charge. The magnitude of $^{15}(V/K)$ reflects the amount of negative charge on the leaving group in the transition state. This KIE results from delocalization of charge arising from the P–O bond fission, which involves the nitrogen via resonance. This KIE reaches a maximum of ~1.003 for transition states with extensive P–O bond fission and no charge neutralization (35). The negligible $^{15}(V/K)$ observed indicates that efficient charge neutralization occurs in the transition state. The $^{18}(V/K)_{bridge}$ is a measure of P–O bond fission. A large normal value indicates extensive P–O bond weakening and can reach 1.03 for a loose transition state with extensive bond fission (35). The $^{18}(V/K)_{bridge}$ KIE also reflects an inverse contribution from protonation. The equilibrium isotope effect for protonation of nitrophenol is 0.985 (58), so a transition state where P–O fission and protonation are both far advanced would show a KIE of about 1.015. PTP reactions show $^{18}(V/K)_{bridge}$ KIEs close to this value. The secondary isotope effect $^{18}(V/K)_{nonbridge}$ reveals changes in bonding to the phosphoryl group (metaphosphate-like or phosphorane-like) in the transition state. This KIE is small and inverse for metaphosphate-like transition states and is normal for more associative reactions (35). Abolishment of general acid catalysis in PTPs is accompanied with increase of the $^{15}(V/K)$ KIE. The magnitude of $^{18}(V/K)_{bridge}$ increases as well, due to the absence of the inverse contribution from protonation (see the entry for the D356A mutant of YopH) (36).

The experimental and most theoretical results indicate that the Michaelis complex consists of the dianion form of the substrate, with the nucleophilic cysteine in the thiolate form and the conserved Asp residue on the WPD-loop in the protonated form, followed by a loose metaphosphate-like phosphoryl transfer in which the leaving group is fully neutralized (2, 36, 59–62), although some theoretical studies have suggested that PTPs utilize the monoanionic form of the substrate (63, 64).

Crystal Structures

An optimal transition state analog would consist of a peptide sequence corresponding to a natural substrate incorporating a tyrosine, with metavanadate (VO_3) poised between the nucleophilic cysteine sulfur atom and the tyrosine hydroxyl group. In solution, orthovanadate (VO_4^{3-}) forms vanadate esters with hydroxylic species, and these are found to be substrates for a range of enzymes, including dehydrogenases, isomerases, and aldolases (65). The formation constants of vanadate esters in aqueous solution are on the order of 0.1–0.2 M^{-1} for aliphatic esters and about 3 times larger for aromatic esters (65). One precedent for vanadate ester formation and enzymatic recognition is the reaction between D-glucose and vanadate. D-Glucose contains one primary and several secondary hydroxyl groups that can form vanadate esters. Despite the many species that form in solution, the small amount of glucose-6-vanadate that forms is selectively recognized by glucose-6-phosphate dehydrogenase (66, 67). In the present work, the tyrosyl vanadate ester of the peptide DADEYL was formed by preincubation of

[5] Amino acid position numbers marked as positive and negative (Asp^{-2}, Leu^{+1}, etc.) represent positions on the peptide relative to Tyr(P).

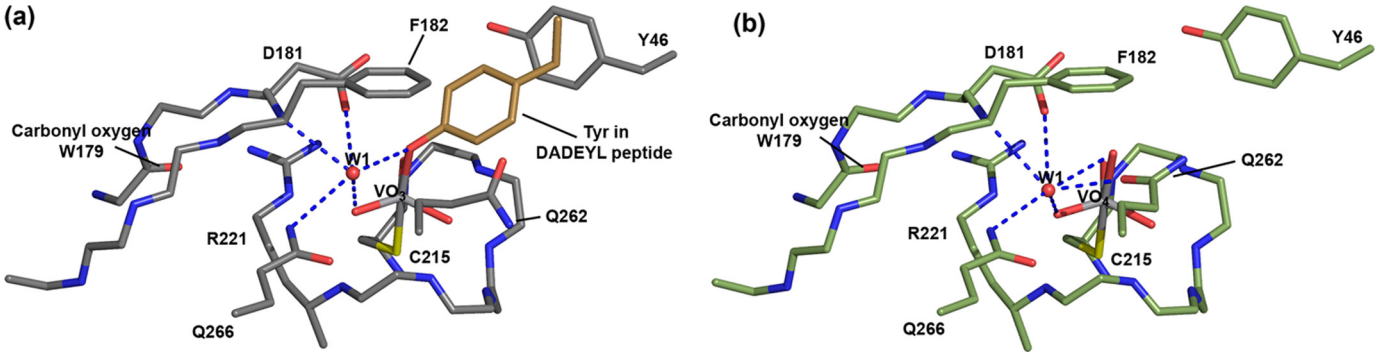

FIGURE 4. **Coordination shell of the water W1 in the active site of PTP1B.** *a*, first transition state; *b*, second transition state. Stereo images of *a* and *b* are included in supplemental Fig. S5.

orthovanadate and peptide and was subsequently bound by PTP1B and co-crystallized.

Vanadate anions form stable tetrahedral structures in solution but exhibit clear preference for trigonal bipyramidal structures in the presence of polydentate ligands (65), including the active site of enzymes, such as PTPs (20, 22). In these enzymes, vanadate exhibits K_i values ranging from 0.4 to 5 μM (23, 68, 69) and structural characteristics resembling the trigonal bipyramidal transition state in phosphoryl transfer reactions. This geometry is formed by nucleophilic attack of the cysteine (Cys^{215} in PTP1B) on the vanadium atom, with the nucleophilic sulfur and leaving group oxygen occupying apical positions. The equatorial oxygen atoms of this structure extensively interact with the P-loop (Fig. 2). The binding mode of vanadate in the active site of PTPs has been considered a fair structural transition state analog, showing clear advantages in relation to other anions (24). For example, tetrahedral anions that do not undergo similar stabilization in the active site of PTPs, exhibit weaker inhibition. The K_i values for phosphate and arsenate range from 10 to 30 mM (62, 70), and K_i values for tungstate range from 5 to 60 μM (70, 71). It has been noted that in some instances, PTP complexes with vanadate resemble a more associative structure than the dissociative TS determined experimentally (68).

Information from the Crystal Structures

Binding of Substrate and Water Molecules in the Active Site

Substrate binding to PTPs is accompanied by the expulsion of several water molecules from the active site. Three water molecules are commonly found in crystal structures of apo-PTPs at positions occupied by the phosphoryl nonbridge oxygens when substrate is bound (31). Displacement of these waters may supply the entropic driving force assisting the substrate binding. Other water molecules have important roles in catalysis by PTP1B (29). The water molecule W1 in Fig. 4 is found in all x-ray structures in the catalytic pathway of PTP1B and is also observed in other members of the PTP family (*e.g. Yersinia* PTP (72) and PTPβ (22)). In TSA1, the coordination shell for W1 includes the side chains of Asp^{181} and Gln^{266}, the backbone amide proton of Phe^{182} in the WPD-loop, and axial and equatorial oxygens of the trigonal bipyramid structure. In TSA2, the coordination shell of W1 also includes the side chain of Gln^{262}. In view of the short distance between the side chain of general acid catalyst Asp^{181} and the oxygen leaving group in the substrate, it is difficult to say that the water molecule W1 is involved in any proton transfer during catalysis. However, this water molecule may be an important structural component of the active site through hydrogen bonding with key side chains. Additionally, this water may be an energy sink by partially solvating the phosphate moiety in the active site. It is important to point out that Gln^{262} and Gln^{266}, both in the coordination shell of water W1, are highly conserved residues in PTPs.

Each crystal structure depicted in Fig. 3 represents a discrete form of PTP1B in the ping-pong mechanism. Next, we provide a step-by-step description of structural changes associated with binding and catalysis.

Changes Accompanying Conversion of the Apoenzyme (PDB Entry 2CM2) to the Michaelis Complex (MC) (PDB Entry 1PTU)

P-loop—Substrate binding to the P-loop occurs with side chain rotation of Arg^{221}, which is rotated by $-71°$ around χ-3. New hydrogen bonds are formed with the phosphate moiety of the substrate, and with the carbonyl oxygen of Trp^{179}. This interaction stabilizes the WPD-loop in the active, closed conformation.

WPD-loop—The closed position of this loop brings the general acid Asp^{181} into position for catalysis (19, 46). Stabilization of the closed conformation is further achieved by interaction of the Phe^{182} side chain with the phosphotyrosine ring of the substrate. Phe^{182} and the highly conserved Tyr^{46} flank the phenyl ring of the substrate.

Q-loop—The Gln^{262} residue occupies the same position in both structures. Steric constraints in the MC prevent the Gln^{262} side chain from interactions with the active site, precluding a catalytic function in the first catalytic step. The side chain is in sufficient proximity to participate in van der Waals interactions with the Tyr(P) side chain of the substrate.

Lys-loop—Lys^{120} is rotated $-100°$ around the χ-4 angle. In the apo structure, the ammonium moiety is embedded in a polar environment interacting with the hydroxyl groups of Ser^{118}, Ser^{216}, and Tyr^{46}. In the MC, the Lys^{120} side chain hydrogen-bonds to the Asp^{181} and Glu^{115} side chains.

Tyr(P) Recognition Loop—The position of Asp^{48} is similar for the apo and MC states, but in the MC, the Asp^{48} side chain hydrogen-bonds to the peptide main chain amides of Tyr(P) and Leu^{+1}. Peptide binding has a strong influence in the position of Arg^{47}, which moves to make hydrogen bonds with Glu^{-1} and the main chain carbonyl of Asp^{-4}.

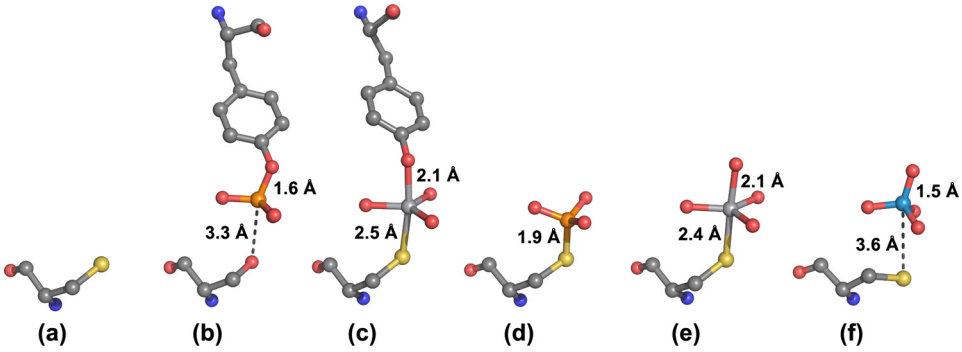

FIGURE 5. **Close-up of details from crystal structures along the reaction pathway catalyzed by PTP1B.** *a*, initial state, apoenzyme; *b*, Michaelis complex; *c*, first transition state; *d*, phosphoenzyme; *e*, second transition state; *f*, product complex. The figure was prepared from superimposed structures, which are presented *side by side*. In the first step, the phosphorus atom swings from the substrate to the nucleophilic cysteine, whereas the positions of the leaving group oxygen, the nucleophile, and nonbridging oxygens do not change appreciably.

Changes Accompanying Conversion of the MC (PDB Entry 1PTU) to the Transition State Analog of the First Step, TSA1 (PDB Entry 3I7Z)

The TSA1 structure depicts a pentacoordinate species consisting of a planar metavanadate with apical ligands and equatorial oxygen atoms interacting with the P-loop. This structure models the TS of the first catalytic step.

P-loop—The Cys^{215} sulfur attacks the vanadyl center *in line* with leaving group departure. The nonbridge oxygen positions are not appreciably different from their position in the MC, but the vanadium position has moved relative to that of phosphorus. The unusually low pK_a of 4.6 for the Cys^{215} thiol (73, 74) results in part from a stabilizing hydrogen bond with Ser^{222}. The sulfur-oxygen distance establishing this interaction is not significantly different in the apo (3.2 Å), MC (3.0 Å) (this is shorter because PDB entry 1PTU is a C215S mutant), and TSA1 (3.3 Å) structures. The constancy of this distance indicates that the low pK_a of the nucleophile is permanently built into the enzymatic structure.

WPD-loop—The Asp^{181} carboxyl group moves closer to the Tyr(P) leaving group oxygen (2.6 Å) than in the MC structure (3.5 Å). This distance is 3.0 Å in a related MC structure (PDB entry 1G1G) with the peptide sequence ETDYpYRKGGKLL bound to an inactive C215A mutant (46). In the first catalytic step, the phosphotyrosine is attacked by the nucleophilic Cys^{215} accompanied by proton transfer from Asp^{181} to the leaving group oxygen. KIE data confirm that the efficiency of leaving group protonation is such that the leaving group is fully neutralized in the TS.

Comparing TSA1 with MC structure (PDB entry 1PTU), the phenyl ring of Phe^{182} is rotated −23° around the χ-1 dihedral; in MC (PDB entry 1G1G), this residue is rotated 15°. The −23° rotation of Phe^{182} permits extensive interaction between the Phe^{182} and the vanadyl tyrosine aromatic rings. However, in the MC 1G1G, the side chain of Arg^{+1} is very close to the Phe^{182} ring, and because of van der Waals or steric clashes, the Phe^{182} assumes a different position compared with MC 1PTU. This variability in the details of peptide-enzyme interactions fits with the substrate flexibility of PTP1B.

Q-loop—The Gln^{262} position does not change appreciably from its position in the MC and remains excluded from proximity with the active site by steric clashes with the vanadyl Tyr. This verifies the proposal of Pannifer *et al.* (29) that Gln^{262} has no catalytic function in the first step.

Lys-loop—The Lys^{120} residue rotates around the χ-4 dihedral by −20°. In both states, this residue hydrogen-bonds to Asp^{181} and Glu^{115}. However, the interaction in the TSA1 seems to be more favorable than in the MC; donor-acceptor distances involving Lys^{120} are 2.6 Å with Asp^{181} and 2.7 Å with Glu^{115} but 0.2–0.3 Å longer in the MC (PDB entry 1PTU). In the other Michaelis complex (PDB entry 1G1G), Lys^{120} is found in a similar position as PDB entry 1PTU and does not exhibit hydrogen bonds as short as those observed in TSA1.

Tyr(P) Recognition Loop—As in other PTP1B structures with bound peptides (PDB entries 1EEO (75), 1G1G, and 1G1H (46)), in TSA1, Asp^{48} forms hydrogen bonds to the main chain amides of vanadyl-Tyr(P) and Leu^{+1} residues. The Asp^{48} residue is conserved among all PTPs and may be important in determining the overall substrate orientation, in positioning the peptide substrate for an optimal orientation for the attack of Cys^{215} and proton transfer from Asp^{181} (46). Our TSA1 structure indicates that this interaction is maintained in the transition state. The Cα position of Asp^{48} moves by 0.5 Å from the MC to the TSA1 structures in order to maintain proper structural requirements for the hydrogen bond between Asp^{48} and the peptide.

The position of Arg^{47} differs from the MC 1PTU by about 3.5 Å in the distal part of the side chain. This is probably related to the bond lengthening of the scissile bond observed from the ground to the transition state (Fig. 5). In the MC, weak hydrogen bonds are present between Arg^{47} and Glu^{-1} and the main chain carbonyl of Asp^{-4} of the peptide. There are no apparent hydrogen bonds involving the Arg^{47} in TSA1, although it is embedded in a position with negative charges from Glu^{-1}, Asp^{-2}, and Asp^{-4}.

The combined changes in the positions of Arg^{47} and Asp^{181} from the ground to the transition state reflect the needs of catalysis. In the transition state, the protein structure at the WPD-loop becomes tighter to facilitate proton transfer but loosens around Arg^{47} in order to permit leaving group departure.

Changes Accompanying Conversion of TSA1 (PDB Entry 3I7Z) to the Phosphoenzyme (PDB Entry 1A5Y)

P-loop—Cys^{215} is phosphorylated. No other significant changes are observed in this region.

WPD-loop—This loop slides horizontally, and Asp^{181} is displaced 1.2 Å relative to its position in TSA1.

Q-loop—A comparison is not possible in this case because PDB entry 1A5Y is a Q262A mutant.

Lys-loop—In the phosphoenzyme, the Lys^{120} side chain is not involved in hydrogen bonds with other protein residues. In TSA1, this residue is involved in hydrogen bonds with Asp^{181}

and Glu^{115}. These interactions may be important for positioning Asp^{181} during catalysis because this residue in the phosphoenzyme is found 1.2 Å away from its catalytically competent position observed in TSA1.

Tyr(P) Recognition Loop—Relative to TSA1, Asp^{48} and Arg^{47} move away from their positions involved in hydrogen bonds with the peptide. This loop backbone is similar to its position in other structures without bound peptide.

Changes Accompanying Conversion of the Phosphoenzyme (PDB Entry 1A5Y) to the Transition State Analog of the Second Step, TSA2 (PDB Entry 3I80)

P-loop—The side chains and backbone positions of TSA1, the phosphoenzyme, and TSA2 are very similar. We note that the hydrogen bonding distances between the Cys^{215} sulfur atom and the oxygen of Ser^{222} (3.3 and 3.2 Å respectively) remain unchanged from those of the apo, MC, and TSA1 structures and are essentially constant through the entire catalytic cycle. In the transition state of the second step, this interaction serves to facilitate the leaving group propensity of the sulfur atom.

WPD-loop—This loop is found in a similar position in TSA1 and TSA2. In the phosphoenzyme structure, the Asp^{181} residue is slightly displaced 1.2 Å away from its position in TSA1 and TSA2. In the second catalytic step, this residue is a general base for the deprotonation of a nucleophilic water molecule.

Q-loop—Comparing TSA2 with TSA1, the Gln^{262} residue is rotated by −120° around the χ-2 angle. This brings the amide moiety into the active site, where it positions the nucleophilic water molecule for phosphoenzyme hydrolysis. This structure explains the observation that the Q262A mutation hinders phosphoenzyme hydrolysis but not the first step of catalysis (29).

Lys-loop—In the phosphoenzyme intermediate, the Lys^{120} side chain is not involved in hydrogen bonds with other protein residues. In TSA2, as in TSA1, Lys^{120} is involved in hydrogen bonds with Asp^{181} and Glu^{115}.

As revealed by the TSA1 and TSA2 structures, the Lys^{120} may interact with key residues in the transition state. This contrasts with molecular dynamics simulations of the ground state, which observed concurrent movements between the WPD-loop and Lys-loop during WPD-loop closure (31). Together, these observations imply that the movement of the Lys-loop probably lags behind the WPD-loop closure in the early stages of each catalytic step.

Tyr(P) Recognition Loop—In TSA2, the side chains of Arg^{47} and Asp^{48} hydrogen bond with each other. The backbone of this region is in a similar position in the phosphoenzyme and TSA2.

The distances between the two apical oxygen atoms are identical within the uncertainty limits of the structure in the two transition state analogs (Fig. 5). This implies a similar transition state for the two phosphoryl transfer reactions.

Changes Accompanying Conversion of TSA2 (PDB Entry 3I80) to the Product Complex (PDB Entry 2HNP)

P-loop and WPD-loop—Both loops return to an open conformation, as observed in the apo enzyme.

Q-loop—Relative to TSA2, in the product complex, Gln^{262} rotates back to the position observed in the apo form.

Lys-loop—In contrast to TSA1 and TSA2, in the intermediate and the product complexes, Lys^{120} is positioned away from Asp^{181} and Glu^{115} and does not hydrogen-bond to protein residues.

Tyr(P) Recognition Loop—The interactions between residues Arg^{47} and Asp^{48} in TSA2 are lost in the product complex.

Complementing these specific step-by-step observations, we also notice that several precedents from the modeling of enzymatic features in small molecules indicate that decreased entropy and proximity have a profound effect in nucleophilic attack and general acid catalysis. In both cases, these effects have shown catalytic contributions of over 10^6-fold (76–78), which, combined, may partially explain the catalytic proficiency of enzymes. Upon formation of the Michaelis complex in PTPs, WPD-loop closure and the resulting proximity of the Asp^{181} side chain to the leaving group oxygen cause the pK_a of the leaving group tyrosine to drop below its acidity in water. It is interesting to observe that lengthening of the scissile P–O bond causes the peptide chain to slightly shift in the active site of PTP1B in TSA1 relative to the MC structure. This change probably occurs upon transformation of the Michaelis complex to the transition state because the apical bond in the trigonal bipyramidal transition state is longer than the respective bond in the ground state. However, the phosphotyrosine ring (and consequently the leaving group oxygen) and nucleophile (Cys^{215}) do not appreciably change their position (Fig. 5). The major part of the reaction coordinate, implied by these structures, is movement of the phosphorus atom between the leaving group and the nucleophile.

The proximity of the general acid in TSA1, brought into the active site by the conformational change associated with WPD-loop closure, implies that the electronic effects of proton transfer to the ester oxygen, rather than only structural consequences, are important for the very small leaving group dependence in PTPs. Site-directed mutagenesis and Brönsted relationships for YopH, another member of the PTP family, show that abolishment of general acid catalysis by Asp is accompanied by a change of the Brönsted β_{lg} from about −0.1 in the wild type to −1 in mutants (70). In the transition state, the general acid catalyst Asp^{181} may drive the proton transfer causing the P–O bond lengthening. The charge in the phosphate moiety changes from −2 in the substrate to approximately −1 in the transition state. Negatively charged nucleophiles are unlikely to react with phosphate monoesters in the dianion form. However, this has been observed in cases where, as in the PTP1B reaction, proton transfer is present or the phosphate moiety is neutral or monoanionic (78).

CONCLUSIONS

The close similarity of the apical O–O distances in TSA1 and TSA2 support the notion that the transition states of the two catalytic steps are very similar. KIE and linear free energy relationship data have suggested that the first TS is loose for the related PTPs, YopH and Stp (36, 62, 79), as is the second TS in Stp1 (80). Because PTPs exhibit very similar active sites, it is likely that the same is true in the transition states of reactions catalyzed by other PTP family members.

Several general conclusions are revealed by the step-by-step analysis. The leaving group propensity in the first catalytic step is modulated by Asp^{181} through an interaction that is controlled by motions of a protein loop. In contrast, the pK_a of the Cys^{251} thiol (the nucleophile in the first step, the leaving group in the second) is controlled by a hydrogen bond in a fixed structural element that is unchanged throughout the catalytic cycle. The unusually low pK_a makes catalytic sense in the second step, in which Cys^{215} is a leaving group. The first step would logically be assisted by a weakened hydrogen bond that would raise this pK_a, but the evidence from the structures is that the low pK_a is fixed. Lys^{120} hydrogen-bonds to key residues involved in catalysis, but its main function may remain in structural and protein-protein interactions. This may be an important factor for development of PTP inhibitors. The transition states of the two catalytic steps are indicated to be essentially identical. A structural rationale for the role of Gln^{262} in the second catalytic step, but not the first, is now evident.

Acknowledgment—We thank Dr. N. K. Tonks for providing the plasmid encoding the wild type PTP1B.

REFERENCES

1. Barford, D., Das, A. K., and Egloff, M. P. (1998) *Annu. Rev. Biophys. Biomol. Struct.* **27,** 133–164
2. Zhang, Z. Y. (1998) *Crit. Rev. Biochem. Mol. Biol.* **33,** 1–52
3. Alonso, A., Sasin, J., Bottini, N., Friedberg, I., Friedberg, I., Osterman, A., Godzik, A., Hunter, T., Dixon, J., and Mustelin, T. (2004) *Cell* **117,** 699–711
4. Hunter, T. (2000) *Cell* **100,** 113–127
5. Elchebly, M., Payette, P., Michaliszyn, E., Cromlish, W., Collins, S., Loy, A. L., Normandin, D., Cheng, A., Himms-Hagen, J., Chan, C. C., Ramachandran, C., Gresser, M. J., Tremblay, M. L., and Kennedy, B. P. (1999) *Science* **283,** 1544–1548
6. Zhang, S., and Zhang, Z. Y. (2007) *Drug Discov. Today* **12,** 373–381
7. Johnson, T. O., Ermolieff, J., and Jirousek, M. R. (2002) *Nat. Rev. Drug Discov.* **1,** 696–709
8. Haj, F. G., Markova, B., Klaman, L. D., Bohmer, F. D., and Neel, B. G. (2003) *J. Biol. Chem.* **278,** 739–744
9. Zhang, Z. Y. (2002) *Annu. Rev. Pharmacol. Toxicol.* **42,** 209–234
10. Ostman, A., Hellberg, C., and Böhmer, F. D. (2006) *Nat. Rev. Cancer* **6,** 307–320
11. Bialy, L., and Waldmann, H. (2005) *Angew. Chem. Int. Ed. Engl.* **44,** 3814–3839
12. DeVinney, R., Steele-Mortimer, O., and Finlay, B. B. (2000) *Trends Microbiol.* **8,** 29–33
13. Nandan, D., and Reiner, N. E. (2005) *Clin. Immunol.* **114,** 266–277
14. Rye, C. S., and Baell, J. B. (2005) *Curr. Med. Chem.* **12,** 3127–3141
15. Shen, K., Keng, Y. F., Wu, L., Guo, X. L., Lawrence, D. S., and Zhang, Z. Y. (2001) *J. Biol. Chem.* **276,** 47311–47319
16. Lad, C., Williams, N. H., and Wolfenden, R. (2003) *Proc. Natl. Acad. Sci. U.S.A.* **100,** 5607–5610
17. Wolfenden, R. (1978) in *Transition States of Biochemical Processes* (Gandour, R. D., and Schowen, R. L., eds) pp. 555–578, Plenum Press, New York
18. Pedersen, A. K., Guo, X. L., Møller, K. B., Peters, G. H., Andersen, H. S., Kastrup, J. S., Mortensen, S. B., Iversen, L. F., Zhang, Z. Y., and Møller, N. P. (2004) *Biochem. J.* **378,** 421–433
19. Jia, Z., Barford, D., Flint, A. J., and Tonks, N. K. (1995) *Science* **268,** 1754–1758
20. Brandão, T. A., Robinson, H., Johnson, S. J., and Hengge, A. C. (2009) *J. Am. Chem. Soc.* **131,** 778–786
21. Denu, J. M., Lohse, D. L., Vijayalakshmi, J., Saper, M. A., and Dixon, J. E. (1996) *Proc. Natl. Acad. Sci. U.S.A.* **93,** 2493–2498
22. Evdokimov, A. G., Pokross, M., Walter, R., Mekel, M., Cox, B., Li, C., Bechard, R., Genbauffe, F., Andrews, R., Diven, C., Howard, B., Rastogi, V., Gray, J., Maier, M., and Peters, K. G. (2006) *Acta Crystallogr. D* **62,** 1435–1445
23. Zhang, M., Zhou, M., Van Etten, R. L., and Stauffacher, C. V. (1997) *Biochemistry* **36,** 15–23
24. Davies, D. R., and Hol, W. G. (2004) *FEBS Lett.* **577,** 315–321
25. Baxter, N. J., Olguin, L. F., Golicnik, M., Feng, G., Hounslow, A. M., Bermel, W., Blackburn, G. M., Hollfelder, F., Waltho, J. P., and Williams, N. H. (2006) *Proc. Natl. Acad. Sci. U.S.A.* **103,** 14732–14737
26. Fauman, E. B., Yuvaniyama, C., Schubert, H. L., Stuckey, J. A., and Saper, M. A. (1996) *J. Biol. Chem.* **271,** 18780–18788
27. Lu, Z., Dunaway-Mariano, D., and Allen, K. N. (2008) *Proc. Natl. Acad. Sci. U.S.A.* **105,** 5687–5692
28. Ala, P. J., Gonneville, L., Hillman, M. C., Becker-Pasha, M., Wei, M., Reid, B. G., Klabe, R., Yue, E. W., Wayland, B., Douty, B., Polam, P., Wasserman, Z., Bower, M., Combs, A. P., Burn, T. C., Hollis, G. F., and Wynn, R. (2006) *J. Biol. Chem.* **281,** 32784–32795
29. Pannifer, A. D., Flint, A. J., Tonks, N. K., and Barford, D. (1998) *J. Biol. Chem.* **273,** 10454–10462
30. Barford, D., Flint, A. J., and Tonks, N. K. (1994) *Science* **263,** 1397–1404
31. Pedersen, A. K., Peters, G. H., Møller, K. B., Iversen, L. F., and Kastrup, J. S. (2004) *Acta Crystallogr. D* **60,** 1527–1534
32. Barford, D., Keller, J. C., Flint, A. J., and Tonks, N. K. (1994) *J. Mol. Biol.* **239,** 726–730
33. Hoff, R. H., Hengge, A. C., Wu, L., Keng, Y. F., and Zhang, Z. Y. (2000) *Biochemistry* **39,** 46–54
34. Cleland, W. W. (2006) in *Isotope Effects in Chemistry and Biology* (Kohen, A., and Limbach, H. H., eds) pp. 915–930, CRC Press, Inc., Boca Raton, FL
35. Hengge, A. C. (2002) *Acc. Chem. Res.* **35,** 105–112
36. Hengge, A. C., Sowa, G. A., Wu, L., and Zhang, Z. Y. (1995) *Biochemistry* **34,** 13982–13987
37. Rigaku Corp. (2006) *CrystalClear: An Integrated Program for the Collection and Processing of Area Detector Data*, Version 1.3.6 SP3 r6, Rigaku Corp., Tokyo
38. McCoy, A. J., Grosse-Kunstleve, R. W., Adams, P. D., Winn, M. D., Storoni, L. C., and Read, R. J. (2007) *J. Appl. Crystallogr.* **40,** 658–674
39. Bailey, S. (1994) *Acta Crystallogr. D* **50,** 760–763
40. Potterton, E., Briggs, P., Turkenburg, M., and Dodson, E. (2003) *Acta Crystallogr. D* **59,** 1131–1137
41. Adams, P. D., Grosse-Kunstleve, R. W., Hung, L. W., Ioerger, T. R., McCoy, A. J., Moriarty, N. W., Read, R. J., Sacchettini, J. C., Sauter, N. K., and Terwilliger, T. C. (2002) *Acta Crystallogr. D* **58,** 1948–1954
42. Painter, J., and Merritt, E. A. (2006) *Acta Crystallogr. D* **62,** 439–450
43. Emsley, P., and Cowtan, K. (2004) *Acta Crystallogr. D* **60,** 2126–2132
44. Davis, I. W., Leaver-Fay, A., Chen, V. B., Block, J. N., Kapral, G. J., Wang, X., Murray, L. W., Arendall, W. B., 3rd, Snoeyink, J., Richardson, J. S., and Richardson, D. C. (2007) *Nucleic Acids Res.* **35,** W375–W383
45. DeLano, W. L. (2007) *The PyMOL Molecular Graphics System*, Version 1.0r2, DeLano Scientific LLC, Palo Alto, CA
46. Salmeen, A., Andersen, J. N., Myers, M. P., Tonks, N. K., and Barford, D. (2000) *Mol. Cell* **6,** 1401–1412
47. Schubert, H. L., Fauman, E. B., Stuckey, J. A., Dixon, J. E., and Saper, M. A. (1995) *Protein Sci.* **4,** 1904–1913
48. Andersen, H. S., Iversen, L. F., Jeppesen, C. B., Branner, S., Norris, K., Rasmussen, H. B., Møller, K. B., and Møller, N. P. (2000) *J. Biol. Chem.* **275,** 7101–7108
49. Guo, X. L., Shen, K., Wang, F., Lawrence, D. S., and Zhang, Z. Y. (2002) *J. Biol. Chem.* **277,** 41014–41022
50. Andersen, J. N., Mortensen, O. H., Peters, G. H., Drake, P. G., Iversen, L. F., Olsen, O. H., Jansen, P. G., Andersen, H. S., Tonks, N. K., and Møller, N. P. (2001) *Mol. Cell. Biol.* **21,** 7117–7136
51. Li, S., Depetris, R. S., Barford, D., Chernoff, J., and Hubbard, S. R. (2005) *Structure* **13,** 1643–1651
52. Melander, L., and Saunders, W. H. (1987) *Reaction Rates of Isotopic Molecules*, pp. 1–3, Robert E. Krieger, Malabar, FL
53. Du, X., and Sprang, S. R. (2009) *Biochemistry* **48,** 4538–4547
54. Humphry, T., Forconi, M., Williams, N. H., and Hengge, A. C. (2004)

J. Am. Chem. Soc. **126,** 11864–11869
55. Humphry, T., Iyer, S., Iranzo, O., Morrow, J. R., Richard, J. P., Paneth, P., and Hengge, A. C. (2008) *J. Am. Chem. Soc.* **130,** 17858–17866
56. Zalatan, J. G., Catrina, I., Mitchell, R., Grzyska, P. K., O'brien, P. J., Herschlag, D., and Hengge, A. C. (2007) *J. Am. Chem. Soc.* **129,** 9789–9798
57. Jones, J. P., Weiss, P. M., and Cleland, W. W. (1991) *Biochemistry* **30,** 3634–3639
58. Hengge, A. C., and Hess, R. A. (1994) *J. Am. Chem. Soc.* **116,** 11256–11263
59. Alhambra, C., Wu, L., Zhang, Z. Y., and Gao, J. (1998) *J. Am. Chem. Soc.* **120,** 3858–3866
60. Asthagiri, D., Dillet, V., Liu, T., Noodleman, L., Van Etten, R. L., and Bashford, D. (2002) *J. Am. Chem. Soc.* **124,** 10225–10235
61. Jackson, M. D., and Denu, J. M. (2001) *Chem. Rev.* **101,** 2313–2340
62. Zhang, Y. L., Hollfelder, F., Gordon, S. J., Chen, L., Keng, Y. F., Wu, L., Herschlag, D., and Zhang, Z. Y. (1999) *Biochemistry* **38,** 12111–12123
63. Hansson, T., Nordlund, P., and Aqvist, J. (1997) *J. Mol. Biol.* **265,** 118–127
64. Kolmodin, K., and Aqvist, J. (1999) *FEBS Lett.* **456,** 301–305
65. Crans, D. C., Smee, J. J., Gaidamauskas, E., and Yang, L. Q. (2004) *Chem. Rev.* **104,** 849–902
66. Drueckhammer, D. G., Durrwachter, J. R., Pederson, R. L., Crans, D. C., Daniels, L., and Wong, C. H. (1989) *J. Org. Chem.* **54,** 70–77
67. Nour-Eldeen, A. F., Craig, M. M., and Gresser, M. J. (1985) *J. Biol. Chem.* **260,** 6836–6842
68. Deng, H., Callender, R., Huang, Z., and Zhang, Z. Y. (2002) *Biochemistry* **41,** 5865–5872
69. Huyer, G., Liu, S., Kelly, J., Moffat, J., Payette, P., Kennedy, B., Tsaprailis, G., Gresser, M. J., and Ramachandran, C. (1997) *J. Biol. Chem.* **272,** 843–851
70. Keng, Y. F., Wu, L., and Zhang, Z. Y. (1999) *Eur. J. Biochem.* **259,** 809–814
71. Stuckey, J. A., Schubert, H. L., Fauman, E. B., Zhang, Z. Y., Dixon, J. E., and Saper, M. A. (1994) *Nature* **370,** 571–575
72. Phan, J., Lee, K., Cherry, S., Tropea, J. E., Burke, T. R., Jr., and Waugh, D. S. (2003) *Biochemistry* **42,** 13113–13121
73. Guan, K. L., and Dixon, J. E. (1991) *J. Biol. Chem.* **266,** 17026–17030
74. Zhang, Z. Y., and Dixon, J. E. (1993) *Biochemistry* **32,** 9340–9345
75. Sarmiento, M., Puius, Y. A., Vetter, S. W., Keng, Y. F., Wu, L., Zhao, Y., Lawrence, D. S., Almo, S. C., and Zhang, Z. Y. (2000) *Biochemistry* **39,** 8171–8179
76. Orth, E. S., Brandão, T. A., Milagre, H. M., Eberlin, M. N., and Nome, F. (2008) *J. Am. Chem. Soc.* **130,** 2436–2437
77. Brandão, T. A., Orth, E. S., Rocha, W. R., Bortoluzzi, A. J., Bunton, C. A., and Nome, F. (2007) *J. Org. Chem.* **72,** 3800–3807
78. Kirby, A. J., Dutta-Roy, N., da Silva, D., Goodman, J. M., Lima, M. F., Roussev, C. D., and Nome, F. (2005) *J. Am. Chem. Soc.* **127,** 7033–7040
79. Hengge, A. C., Zhao, Y., Wu, L., and Zhang, Z. Y. (1997) *Biochemistry* **36,** 7928–7936
80. Zhao, Y., and Zhang, Z. Y. (1996) *Biochemistry* **35,** 11797–11804